ARTICLE

Single-Entity Electroanalysis

Platinum Nanoparticle-based Collision Electrochemistry for Rapid Detection of Breast Cancer MCF-7 Cells

Fu-Xing Qin, Ming-Ke Li, Hui-Long Zhou, Wei Wen, Xiu-Hua Zhang, Sheng-Fu Wang, Zhen Wu*

Hubei Key Laboratory for Precision Synthesis of Small Molecule Pharmaceuticals & Ministry of Education Key Laboratory for the Synthesis and Application of Organic Functional Molecules & College of Chemistry and Chemical Engineering, Hubei University, Wuhan, 430062, PR China

Abstract

Cancer metastasis is the leading cause of death in cancer patients worldwide and one of the major challenges in treating cancer. Circulating tumor cells (CTCs) play a pivotal role in cancer metastasis. However, the content of CTCs in peripheral blood is minimal, so the detection of CTCs in real samples is extremely challenging. Therefore, efficient enrichment and early detection of CTCs are essential to achieve timely diagnosis of diseases. In this work, we constructed an innovative and sensitive single-nanoparticle collision electrochemistry (SNCE) biosensor for the detection of MCF-7 cells (human breast cancer cells) by immunomagnetic separation technique and liposome signal amplification strategy. Liposomes embedded with platinum nanoparticles (Pt NPs) were used as signal probes, and homemade gold ultramicroelectrodes (Au UME) were used as the working electrodes. The effective collision between Pt NPs and UME would produce distinguishable step-type current. MCF-7 cells were accurately quantified according to the relationship between cell concentration and collision frequency (the number of step-type currents generated per unit time), realizing highly sensitive and specific detection of MCF-7 cells. The SNCE biosensor has a linear range of 10 cells·mL^{-1} to 10^5 cells·mL^{-1} with a detection limit as low as 5 cells·mL^{-1}. In addition, the successful detection of MCF-7 cells in complex samples showed that the SNCE biosensors have great potential for patient sample detection.

Keywords: Circulating tumor cells; Single-nanoparticle collision electrochemistry; Immunomagnetic separation; Liposome; Platinum nanoparticles

1. Introduction

Single-nanoparticle collision electrochemistry (SNCE) has become an efficient analytical method because of its high throughput and high sensitivity [1−3]. In SNCE experiments, single nanoparticles (NPs), driven by Brownian motion, diffuse onto the surface of an ultramicroelectrode (UME) and collide with it to generate transient currents [4−7]. The physicochemical properties of individual NPs can be obtained by analyzing the collision frequency, peak shape, and peak current intensity [8−11]. For example, Zhang et al. developed the current lifetime-based SNEC sensor that could *in-situ* monitor agglomeration/aggregation of individual small size NPs, providing effective guidance for practical applications of nanomaterials [12]. Meanwhile, SNCE technology has great potential for application in the area of bioanalysis and detection because of its advantages of low sample consumption, fast response time and low cost [13−18]. Previously, hindered SNCE was used to directly detect biological entities [19,20] and non-biological particles [21,22]. For example, Kim et al.

Received 29 April 2024; Received in revised form 5 June 2024; Accepted 8 June 2024
Available online 9 June 2024

* Corresponding author, Zhen Wu, E-mail address: wuzhen@hubu.edu.cn.

https://doi.org/10.61558/2993-074X.3483

found that when red blood cells (RBCs) were introduced into the electrolyte, they would attach to the electrode surface, and thus the mass transfer of ferrous cyanide to the electrode was blocked, resulting in a decrease in the steady-state current, which enabled the detection of RBCs [23]. However, irreversible adhesion of impurities would poison the electrode, and non-target substances would also collide with the microelectrode to generate signals. The specificity of hindered SNCE is low. Therefore, the sensitivity and specificity of SNCE may be greatly improved by converting the detection of bioanalyte into the detection of electroactive NPs employing electrocatalytic or self-electrolytic. For instance, Li's group had developed a size-resolved biosensor based on the catalytic oxidation of hydrazine hydrate (N_2H_4) by Pt NPs, which exploited differences in the shape of the current in a single run to allow for multiple immunoassays of miRNAs in a single run [17].

Cancer metastasis refers to the separation of CTCs from the primary tumor into the circulatory system to form new tumors in other locations in the body [24—27]. This process leads to the death of a large number of cancer patients. CTCs have been identified as important biomarkers for diagnostic and prognostic assessments and for monitoring responses to therapy [28—31]. Due to the rarity and heterogeneity of CTCs, reliable techniques are required for effective enrichment and detection [32]. Currently, the enrichment methods of CTCs are broadly categorized by physical selection methods (size and density) and immunoaffinity methods [33—36]. The key technical challenge is how to efficiently capture CTCs in a way that is easy for a subsequent processing and analysis. In recent years, immunomagnetic beads (IMBs) have been widely used to enrich biological samples in immunoassays due to their high capture efficiency and strong anti-interference ability. The application of IMBs in SNCE experiments can improve the sensitivity of biosensors. In this work, human breast cancer cells (MCF-7 cells) cultured *in vitro* were used as the target CTCs for the study.

In this study, we constructed a neoteric SNCE biosensor based on the oxidation of N_2H_4 catalyzed by Pt NPs to generate step-type current transients for rapid identification and detection of MCF-7 cells. The schematic diagram is shown in Scheme 1. The anti-EpCAM antibody-modified IMBs can specifically recognize and capture MCF-7 cells for efficient separation. Biotin-modified, platinum nanoparticle-embedded liposomes (Pt-lip-biotin) with biotin-functionalized aptamers can be connected through specific interactions with streptavidin (SA). The Pt-lip-biotin signaling probes specifically recognized and bound to the EpCAM of MCF-7 cells to form complexes, and rapid rupture of the liposomes in the presence of the surfactant 1 × PBST and released the embedded Pt NPs. The Pt NPs were collected for SNCE experiments, which were performed to establish a relationship between the concentration of MCF-7 cells and the collision frequency of Pt NPs and Au UME, realizing the rapid quantitative detection of MCF-7 cells in the samples.

2. Experimental section

2.1. Materials

L-α-phosphatidylcholine, cholesterol and biotin-coupled phosphoethanolamine (PE-PEG2000-biotin) were purchased from Aladdin Industries, and MBs were purchased from Ademtech. Anti-EpCAM mouse monoclonal antibody (mAb) was

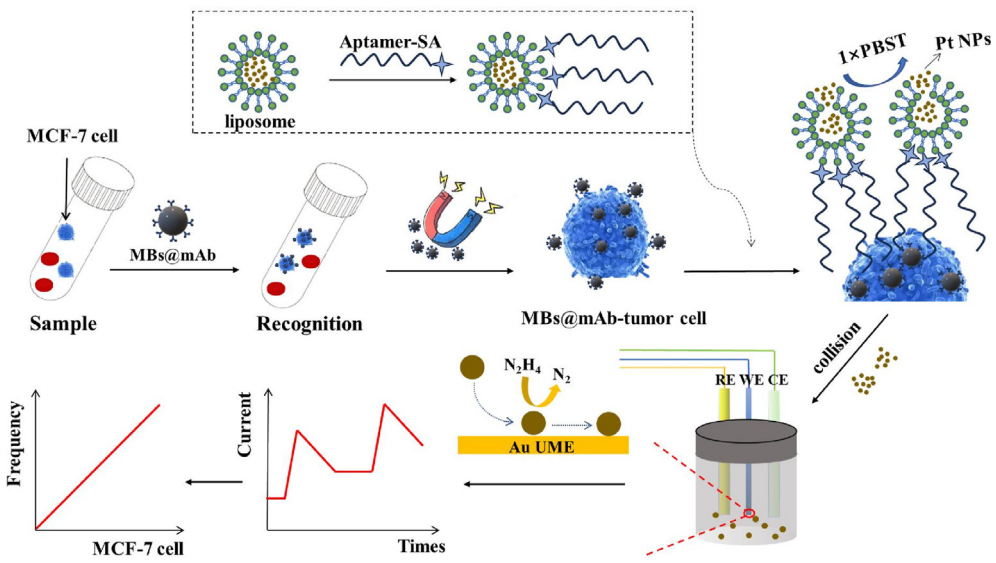

Scheme 1. Schematic representation of the Pt NPs-based SNCE biosensor for detecting MCF-7 cells.

obtained from Beijing Yiqiao Shenzhou Technology Co., Streptavidin was purchased from Promega. Hydrazine hydrate (85%) was purchased from Shanghai Sinopharm Group. 10 × PBST (phosphate buffer containing Tween-20) was purchased from Sangon Biotech (Shanghai) Co., Ltd. Aptamers were provided by Bioengineer Biologics, as shown in Table 1.

Table 1. Sequences of aptamer.

	Sequence (5′−3′)
Apt-Biotin	Biotin-AAA AAA CAC TAC AGA GGT TGC GTC TGT CCC ACG TTG TCA TGG GGG GTT GGC CTG

2.2. Synthesis of Pt NPs

Added 0.2% $H_2PtCl_6 \cdot 6H_2O$ (7.76 mL) to boiling water (100 mL) and boiled for 1 min. Following this, 2.37 mL of 1% $C_6H_5Na_3O_7 \cdot 2H_2O$ and 0.05% $C_6H_5Na_3O_7 \cdot 2H_2O$ were added and boiled for an additional 30 s. Subsequently, added a mixture solution comprising fresh 0.08% $NaBH_4$, 1% $C_6H_5Na_3O_7 \cdot 2H_2O$ and 0.05% $C_6H_8O_7 \cdot H_2O$ (totaling 1.18 mL), and boiled for 10 min to obtain seed Pt NPs (3~4 nm). Next, the Pt NPs seed solution (1.0 mL) was combined with H_2O (29.0 mL) to synthesize a larger volume of Pt NPs at 25 °C. While stirring, 1.25% ascorbic acid solution, 1% $C_6H_5Na_3O_7 \cdot 2H_2O$ solution (totaling 0.5 mL) and 0.5 mol·L^{-1} H_2PtCl_6 solution (0.023 mL) were added. The above solution was then boiled for a total of 30 min to complete the reaction. After cooling to room temperature, dialyzed in water for 24 h.

2.3. Preparation of anti-EpCAM antibody-modified immunomagnetic beads

The IMBs were made biologically functional through the covalent reaction of carboxyl-activated MBs with the amino group of the antibody. First, mAb (200 μL, 5 mg·mL^{-1}) was added to a 10 mmol·L^{-1} PBS solution (pH = 6.8) enriched with EDC (0.05 mol·L^{-1}) and NHS (0.05 mol·L^{-1}), and the reaction was oscillated at 37 °C for 30 min. The reaction mixture was magnetically separated and then washed three times consecutively with 10 mmol·L^{-1} PBS (pH = 7.4). Subsequently, mAb (anti-EpCAM mAb, 0.01 mg·mL^{-1}) was introduced, and the reaction was carried out at 37 °C for 4 h. After another round of three washes with above PBS, BSA (1%) was added to block the unbound sites for 30 min at 37 °C. The IMBs were dissolved in the above PBS and stored at 4 °C.

2.4. Biotin-modified, Pt NPs-embedded liposome (Pt-lip-biotin)

Total volume 1 mL chloroform dissolved L-α-phosphatidylcholine, cholesterol, and biotin-coupled phosphoethanolamine (total 5 mg) at the molar ratio of 40:30:30 and mixed. After rotary evaporation at 40 °C for 5 min, 5 mL of Pt NPs solution was subsequently added to strip the lipid film formed on the inner surface of the vials, and Pt-lip-biotin was formed within 1 h. The milky suspension was introduced into a microextruder containing a polycarbonate membrane (400 nm) to obtain liposomes of uniform diameter (400 nm). The obtained solution was kept for later use after 1.5 h of dialysis.

2.5. High-efficiency capture and accurate quantitative detection of MCF-7 cells

First, IMBs were incubated with peripheral blood samples for 15 min to isolate MCF-7 cells. Subsequently, magnetically separated collected IMBs-cells (1 mL) were incubated with liposome-adaptors for 30 min at 37 °C. To release the Pt NPs from liposomes, 20 μL of 1 × PBST was added within 2 min and then magnetically separated by centrifugation. The SNCE experiments were performed in an electrochemical workstation (CHI 660E). During the experiment, the supernatant containing Pt NPs was introduced into the KCl solution. The collision experiments were carried out using −0.2 V vs. Ag/AgCl (3 mol·L^{-1} KCl) potentials for 500 s.

3. Results and discussion

3.1. Two keys for SNCE: preparing and characterizing Pt NPs and Au UME

Uniformly dispersed NPs and well-performing electrodes are necessary to ensure that the SNCE technique achieves the maximum analytical performance and detects signals at the pA level. In this work, we constructed an outstanding performance SNCE biosensor based on the principle that Pt NPs catalyze the oxidation of N_2H_4 to generate a step-type transient current. The Pt NPs were synthesized by a seed-mediated method [37]. The surface charge of the Pt NPs is negative (Fig. S1). It can be seen from Fig. 1(a) that the Pt NPs were flower-shaped and evenly dispersed. In Fig. 1(b), the size of Pt NPs was approximately 24 ± 4 nm. The concentration of the synthesized Pt NPs was approximately 292 pmol·L^{-1} as determined by UV-vis absorbance method (see Supporting Information S2).

In the SNCE experiments, the performance of the electrodes also has a non-negligible impact on

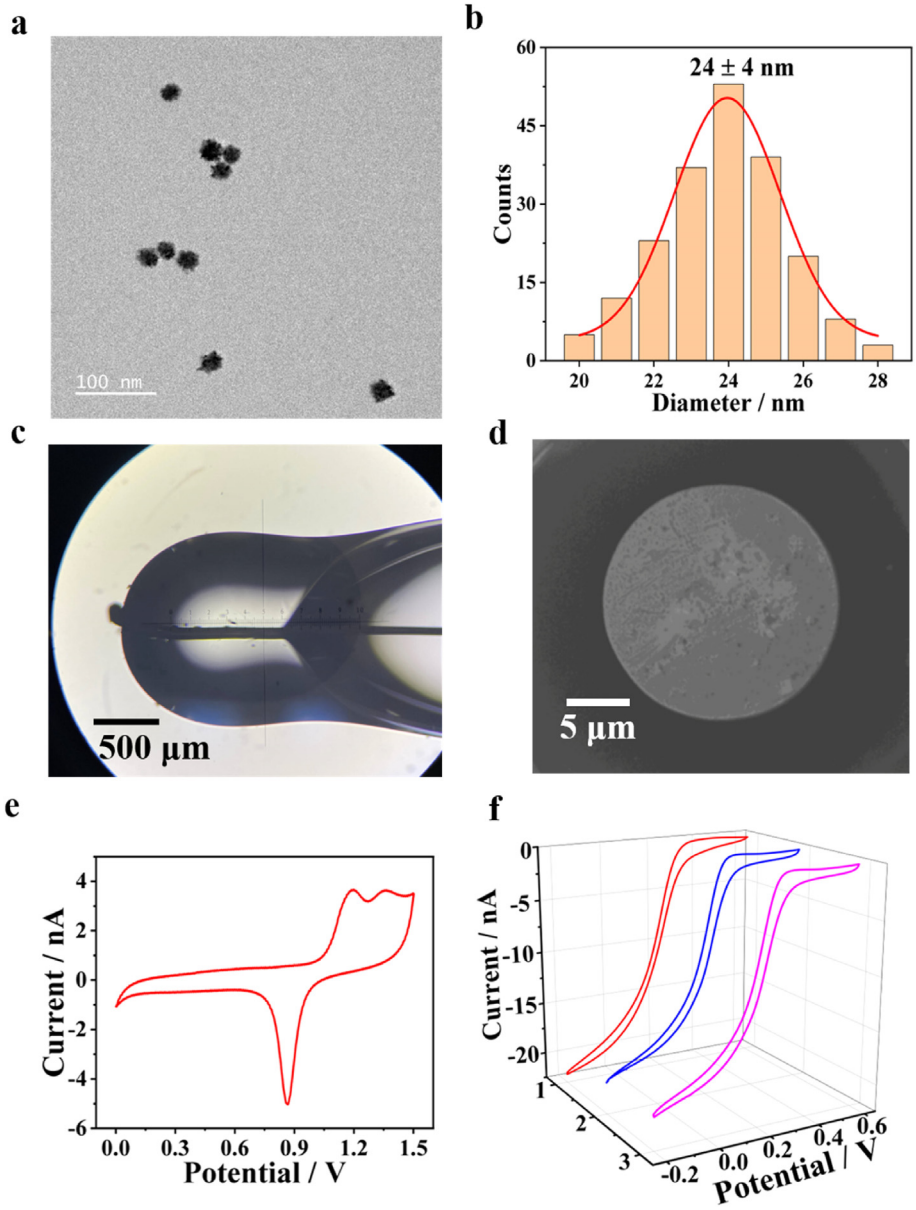

Fig. 1. (a) TEM image of Pt NPs; (b) Statistical graph of particle size of Pt NPs; (c) Micrograph of the prepared Au UME; (d) SEM image of the surface of the gold wire after polishing and cleaning; (e) CV curvw of homemade Au UME in H_2SO_4 (0.5 mol·L^{-1}); (f) Homemade Au UME differential exploration.

the experiment. The preparation process of the Au UME used in this study is shown in Fig. S3. Fig. 1(c) is an optical microscopic image of the Au UME, which clearly shows that the inside of the Au UME was very clean with no liquid leakage and no bending of the gold wire. Fig. 1(d) is SEM image of Au UME, which shows that even after polishing, the Au UME still maintained its original disc structure. Therefore, the homemade UME could be reused after activation, thus saving material and preparation time. The Au UME was polished using a polishing cloth and polishing powder, and then placed in 0.5 mol·L^{-1} sulfuric acid and 5 mmol·L^{-1} $K_3[Fe(CN)]_6$ (containing 0.1 mol·L^{-1} KCl) solutions separately for cyclic voltammetric (CV) scanning. As shown in Fig. 1(e), redox peaks were observed at the corresponding positions in the CV test performed in 0.5 mol·L^{-1} H_2SO_4, which proves that the Au UME had been successfully prepared. In addition, in Fig. 1(f), the CV curves were S-shaped with minimal variation between measurements, indicating that the differences between electrodes were negligible. In the Supporting Information S3, we calculated the radius of the homemade Au UME (13.6 µm), which matched the radius of the original gold wire, proving that the preparation of Au UME was successful.

In conclusion, we prepared the uniformly dispersed Pt NPs (24 nm) and well-performed Au UME (13.6 µm) for the SNCE experiments.

3.2. Specific capture of MCF-7 cells by IMBs

In order to isolate MCF-7 cells quickly and efficiently in complex samples, we introduced MBs into the SNCE biosensor. As illustrated in Fig. 2(a and b), TEM images show that MBs had good dispersion. The diameters of 200 MBs were randomly measured, yielding an average size of approximately 434 ± 150 nm. The magnetic frame could capture MBs in 100 s with a capture efficiency of up to 99% (Fig. S4). The anti-EpCAM antibody attached to the MBs surface via an amide bond. This allowed the preparation of IMBs with both immunorecognition and magnetic properties. To verify the specificity and sensitivity of IMBs to different CTCs, we evaluated the capture efficiency of IMBs. Human breast cancer cells (MCF-7) were used as the experimental group, and human cervical cancer cells (Hela), human malignant glioblastoma cells (U87), human umbilical vein endothelial cells (HUVEC), and rat adrenal pheochromocytoma cells (PC-12) were used as the control groups. As demonstrated in Fig. 2(c), different cells were captured using the modified IMBs and unmodified MBs. For the MBs without antibodies, the capture efficiency for these five cells remained low at about 5.0%. However, the capture efficiency of IMBs could reach 89.2% for MCF-7 cells and remained around 5.0% for other interfering cells. The above results indicated that the recognition between IMBs and EpCAM-positive cells was specific and effective.

3.3. Feasibility of Pt NPs-SNCE for bioanalysis

In collision experiments, it was found that the concentration of KCl affected the stability of Pt NPs. As can be seen in Fig. S5, the particle size of Pt hydrated nanoparticles was the smallest in KCl with a concentration of 20 $mmol \cdot L^{-1}$, so 20 $mmol \cdot L^{-1}$ of KCl was chosen. Meanwhile, the type of collision signaling for the N_2H_4 oxidation reaction catalyzed by the Pt NPs was a potential-dependent process. We performed the SNCE tests on Pt NPs at five sets of voltages (i.e., 0 V, −0.05 V, −0.1 V, −0.15 V, and −0.2 V). The results are shown in Fig. 3(a), the more negative the voltage, the higher the collision frequency and the lower the current intensity of the step-type peak. By magnifying individual current signal, as shown in Fig. 3(b), it was evident that the higher the negative voltage, the more pronounced the "step" becomes. This may be due to the increased electrostatic repulsion between the Pt NPs and the electrodes at lower voltages, preventing the particles from moving towards the electrode surface. The gaseous substance of nitrogen produced by the reaction is thought to be responsible for the attenuation of the electrocatalytic current because it blocks the electrocatalytic reaction. Lower voltages lead to faster electrochemical reactions and product generation, but also to faster deactivation rates. In conclusion, we had identified −0.2 V as the optimum voltage for conducting Pt NPs collision experiments. As can be seen in Fig. 3(c), N_2H_4 was hardly oxidized on the Au UME at −0.2 V. However, after the addition of Pt NPs, an obvious transient current appeared at −0.2 V (Fig. 3(d)), which indicated that the oxidation reaction of N_2H_4 occurred in the presence of the catalyst. The results indicated that only in the presence of Pt NPs could N_2H_4 be oxidized at the voltage of −0.2 V. Effective collisions of Pt NPs generated distinguishable step-type transient current signals. The step-type signals were generated mainly due to the adhesion of NPs to the electrode surface after collision with the electrode, and the successive catalysis of the substrate electrode led to the step-type rise of the signals (Fig. S6).

In order to verify the feasibility of the prepared Pt NPs as signaling markers for SNCE experiments, we performed collision experiments using the prepared Pt NPs in a three-electrode system. 100 μL, 200 μL, 300 μL, 400 μL, and 500 μL of Pt NPs solutions were added into 20 $mmol \cdot L^{-1}$ KCl solution to make a total volume of 3.5 mL, and then N_2H_4 (5 μL) was added into the solution to obtain *i-t* curves by collision experiment. It is worth noting that the current fluctuation generated by the collision is large, which may be due to

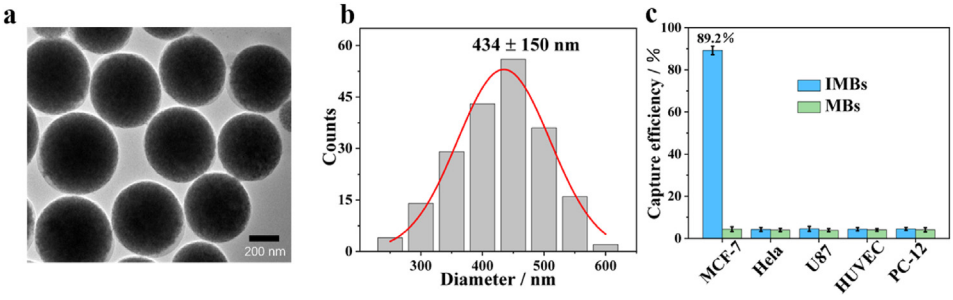

Fig. 2. (a) TEM image of MBs; (b) Particle size statistics of 200 MBs; (c) Capture efficiency graphs of IMBs and MBs on different cells.

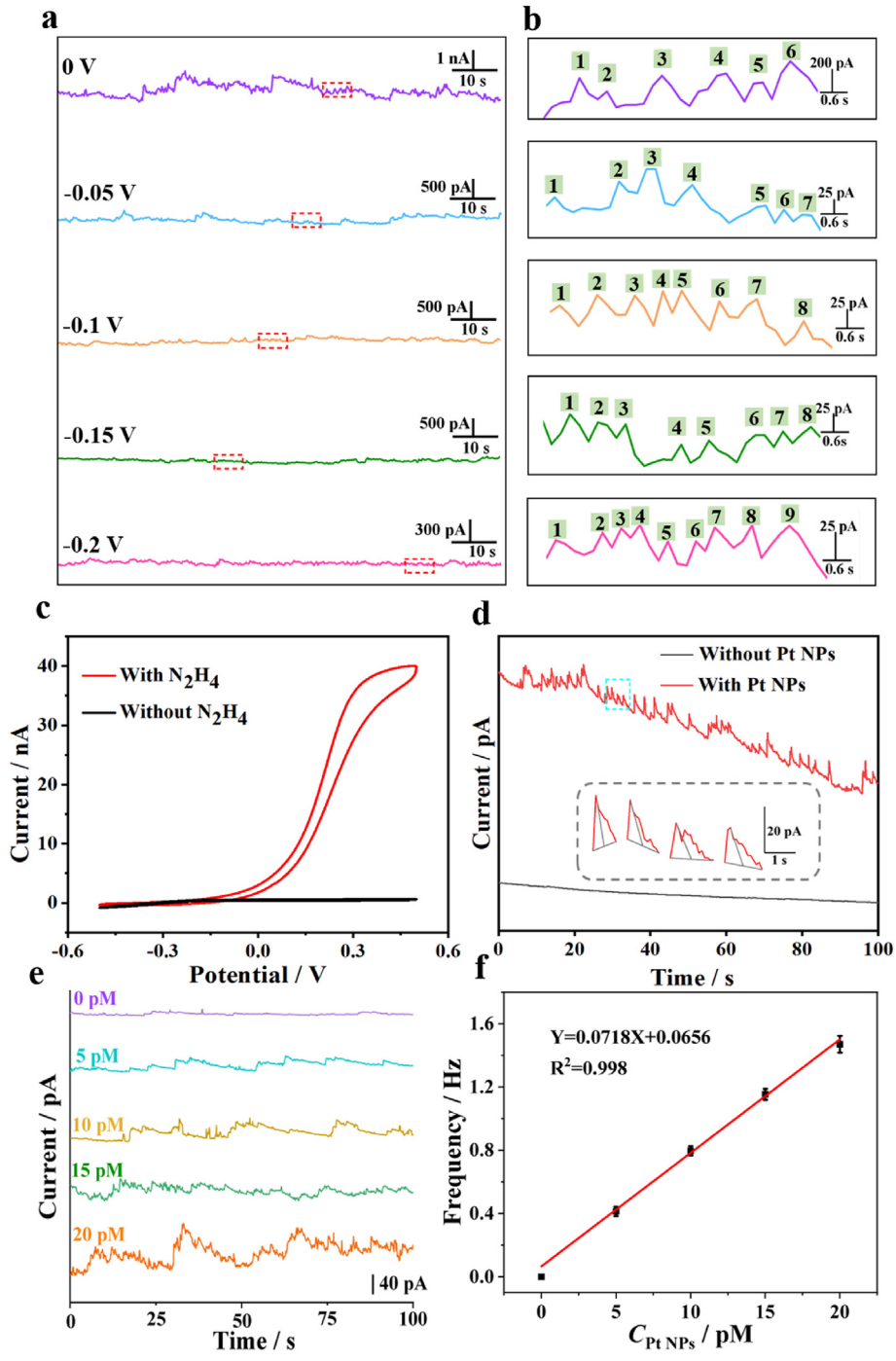

Fig. 3. (a) i-t curves of Pt NPs colliding with Au UME at different applied voltages; (b) Localised magnification in Fig. (a); (c) CV curves of Au UME in 20 mmol·L^{-1} KCl with and without 10 mmol·L^{-1} N_2H_4; (d) i-t curves in KCl containing 10 mmol·L^{-1} N_2H_4, with and without Pt NPs (5 pmol·L^{-1}); (e) i-t curves recorded after collisions of different concentrations of Pt NPs (0, 5, 10, 15, and 20 pmol·L^{-1}) with Au UME; (f) Different concentrations of Pt NPs versus collision frequency.

the inhomogeneity between individual Pt NP and the difference between Au UME. Hence, the SNCE quantification by using collision frequency instead of current intensity is expected to avoid the current fluctuation problem, showing the advantages of SNCE application in analytical detection. In Fig. 3(e), it could be observed very clearly that more and more collision peaks were obtained with the increased concentration of Pt NPs solution. As shown in Fig. 3(f), the concentration of Pt NPs was linearly related to its collision frequency, demonstrating that the prepared Pt NPs could be used as signal markers for SNCE experiments.

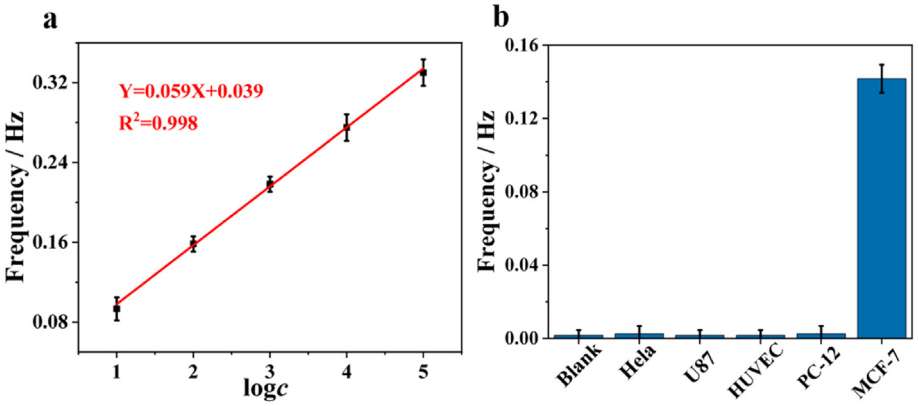

Fig. 4. (a) Collision frequency of Pt NPs is linearly related to the logarithm of cell concentration; (b) Specificity test.

3.4. Quantitative and specific detection of MCF-7 cells

It has been demonstrated that the synthesized Pt NPs could be used to detect MCF-7 cells. Therefore, the cells solutions with concentrations of 10, 10^2, 10^3, 10^4, and 10^5 cells·mL^{-1} were placed in strictly sterilized centrifuge tubes, to which IMBs as well as Pt-lip-biotin linked to aptamers were added. After incubation for 15 min, the obtained MCF-7 cells were enriched in PBS solution by magnetic separation. After adding 1 × PBST to the PBS solution, the magnetic separation was performed again, at this time, the liposomes would be ruptured. The internally embedded Pt NPs would be released into the solution and taken for the collision experiments. The results of three collision experiments were counted, and the obtained relationship is shown in Fig. 4(a). The figure shows that the logarithm of cell concentration is linearly related to the collision frequency, allowing quantification of the MCF-7 cells concentration in the complex samples. As demonstrated in Fig. 4(b), the proposed SNCE biosensor could specifically distinguish MCF-7 cells from other interfering cells, showing the high selectivity of the method.

3.5. Applications in complex samples

In order to investigate the stability in the application of this signal-resolved SNCE, about 300 MCF-7 cells were put into PBS, FBS and serum, separately. After the magnetic separation, the enriched cells were used for SNCE quantification experiments. As shown in Table 2, the *i-t* curves of all corresponding NPs showed significant transient currents and almost similar collision frequency. It indicated that the colliding NPs were almost unaffected in different samples. The relative standard deviation (RSD) values were 5.61%, 4.18% and 4.83% in PBS, FBS and serum, respectively. It proved that the method has good practicality and repeatability. Overall, our constructed SNCE biosensor has great potential in complex sample detection.

Table 2. Statistics of collision frequency in different complex samples.

Sample	Frequency/Hz			Mean	SD	RSD
	1	2	3			
PBS	0.1850	0.1800	0.1700	0.1783	0.0076	5.61%
FBS	0.1800	0.1750	0.1900	0.1817	0.0076	4.18%
Serum	0.1750	0.1750	0.1900	0.1800	0.0087	4.83%

4. Conclusions

In this study, we constructed a novel SNCE biosensor based on step-type currents generated by the catalytic N_2H_4 oxidation of Pt NPs for rapid identification and detection of MCF-7 cells. A signal amplification strategy of liposome embedding and magnetic separation was used. MCF-7 cells were accurately quantified according to the relationship between the cell concentration and collision frequency derived from the SNCE experiments, and a highly sensitive and specific detection of MCF-7 cells (5 cells·mL^{-1}) was achieved. The successful detection of MCF-7 cells in complex samples showed that SNCE biosensors have great potential for patient sample detection.

Conflict of interest

The authors declare no competing interest.

Acknowledgement

This work was supported by the National Natural Science Foundation of China (Nos. 22274037, 22376055 and 21904032), and the Natural Science Foundation of Hubei Province (2022CFB383).

References

[1] Xu W, Zou G Q, Hou H S, Ji X. Single particle electrochemistry of collision[J]. Small, 2019, 15(32): 1804908.

[2] Chen M, Lu S M, Wang H W, Long Y T. Tracking light-induced fragmentation of single silver nanoparticles by single entity electrochemistry[J]. J. Electrochem., 2022, 28(3): 2108521.

[3] Sun L L, Wang W, Chen H Y. Dynamic nanoparticle-substrate contacts regulate multi-peak behavior of single silver nanoparticle collisions[J]. Chemelectrochem., 2018, 5(20): 2995−2999.

[4] Oja S M, Robinson D A, Vitti N J, Edwards M A, Liu Y W, White H S, Zhang B. Observation of multipeak collision behavior during the electro-oxidation of single Ag nanoparticles[J]. J. Am. Chem. Soc., 2017, 139(2): 708−718.

[5] Sun L L, Wang W, Chen H Y. Correlated optical imaging and electrochemical recording for studying single nanoparticle collisions[J]. J. Electrochem., 2019, 25(3): 386−399.

[6] Defnet P A, Zhang B. Collision, adhesion, and oxidation of single Ag nanoparticles on a polysulfide-modified microelectrode[J]. J. Am. Chem. Soc., 2021, 143(39): 16154−16162.

[7] Ding Q D, Sun Z H, Ma W. Probing conformational kinetics of catalase with and without magnetic field by single-entity collision electrochemistry[J]. Sci. Bull., 2023, 68(21): 2564−2573.

[8] Zhou M, Wang D, Mirkin M V. Electrochemical evaluation of the number of Au atoms in polymeric gold thiolates by single particle collisions[J]. Anal. Chem., 2018, 90(14): 8285−8289.

[9] Su T, Guo J, He Z K, Zhao J J, Gao Z D, Song Y Y. Single-nanoparticle-level understanding of oxidase-like activity of au nanoparticles on polymer nanobrush-based proton reservoirs[J]. Anal. Chem., 2023, 95(31): 11807−11814.

[10] Guo J, Pan J, Chang S, Wang X W, Kong N, Yang W R, He J. Monitoring the dynamic process of formation of plasmonic molecular junctions during single nanoparticle collisions[J]. Small, 2018, 14(15): 1704164.

[11] Hafez M E, Ma H, Ma W, Long Y T. Unveiling the intrinsic catalytic activities of single-gold-nanoparticle-based enzyme mimetics[J]. Angew Chem. Int. Ed., 2019, 131(19): 6393−6398.

[12] Bai Y Y, Yang Y J, Xu Y, Yang X Y, Zhang Z L. Current lifetime of single-nanoparticle electrochemical collision for in situ monitoring nanoparticles agglomeration and aggregation[J]. Anal. Chem., 2023, 95(9): 4429−4434.

[13] Zhang J H, Zhou Y G. Single particle impact electrochemistry: analyses of nanoparticles and biomolecules[J]. J. Electrochem., 2019, 25(3): 374−385.

[14] Wang H, Yang C, Tang H, Li Y X. Stochastic collision electrochemistry from single G-quadruplex/hemin: electrochemical amplification and microRNA sensing[J]. Anal. Chem., 2021, 93(10): 4593−4600.

[15] Dunevall J, Fathali H, Najafinobar N, Lovric J, Wigstrom J, Cans C S, Ewing A G. Characterizing the catecholamine content of single mammalian vesicles by collision-adsorption events at an electrode[J]. J. Am. Chem. Soc., 2015, 137(13): 4344−4346.

[16] Dick J E. Electrochemical detection of single cancer and healthy cell collisions on a microelectrode[J]. Chem. Commun., 2016, 52(72): 10906−10909.

[17] Qiu X, Dai Q S, Tang H R, Li Y X. Multiplex assays of MicroRNAs by using single particle electrochemical collision in a single run[J]. Anal. Chem., 2023, 95(35): 13376−13384.

[18] Peng M H, Zhou Y G. Impact electrochemical analysis of soft bio-particles: a mini review[J]. Electrochem. Commun., 2023, 150: 107490.

[19] Fosdick S E, Anderson M J, Nettleton E G, Crooks R M. Correlated electrochemical and optical tracking of discrete collision events[J]. J. Am. Chem. Soc., 2013, 135(16): 5994−5997.

[20] Dick J E, Hilterbrand A T, Strawsine L M, Bard A J. Enzymatically enhanced collisions on ultramicroelectrodes for specific and rapid detection of individual viruses[J]. Proc. Natl. Acad. Sci. USA, 2016, 113(23): 6403−6408.

[21] Dick J E, Renault C, Bard A J. Observation of single-protein and DNA macromolecule collisions on ultramicroelectrodes [J]. J. Am. Chem. Soc., 2015, 137(26): 8376−8379.

[22] Deng Z, Elattar R, Maroun F, Renault C. In situ measurement of the size distribution and concentration of insulating particles by electrochemical collision on hemispherical ultramicroelectrodes[J]. Anal. Chem., 2018, 90(21): 12923−12929.

[23] Ho T LT, Hoang N TT, Lee J, Park J H, Kim B K. Determining mean corpuscular volume and red blood cell count using electrochemical collision events[J]. Biosens. Bioelectron., 2018, 110: 155−159.

[24] Alix-Panabières C, Pantel K. Characterization of single circulating tumor cells[J]. FEBS Lett., 2017, 591(15): 2241−2250.

[25] Edd J F, Mishra A, Smith K C, Kapur R, Maheswaran S, Haber D A, Toner M. Isolation of circulating tumor cells[J]. iScience, 2022, 25(8): 104696.

[26] Shen Z Y, Wu A G, Chen X Y. Current detection technologies for circulating tumor cells[J]. Chem. Soc. Rev., 2017, 46(8): 2038−2056.

[27] Ferreira M M, Ramani V C, Jeffrey S S. Circulating tumor cell technologies[J]. Mol. Oncol., 2016, 10(3): 374−394.

[28] Rawal S, Yang Y P, Cote R, Agarwal A. Identification and quantitation of circulating tumor cells[J]. Ann. Rev. Anal. Chem., 2017, 10: 321−343.

[29] Lawrence R, Watters M, Davies C R, Pantel K, Lu Y J. Circulating tumor cells for early detection of clinically relevant cancer[J]. Nat. Rev. Clin. Oncol., 2023, 20(7): 487−500.

[30] Bankó P, Lee S Y, Nagygyörgy V, Zrínyi M, Chae C H, Cho D H, Telekes A. Technologies for circulating tumor cell separation from whole blood[J]. J. Hematol. Oncol., 2019, 12: 1−20.

[31] Ju S W, Chen C, Zhang J H, Xu L, Zhang X, Li Z Q, Chen Y X, Zhou J C, Ji F Y, Wang L B. Detection of circulating tumor cells: opportunities and challenges[J]. Biomark. Res., 2022, 10(1): 58.

[32] Moon D H, Lindsay D P, Hong S, Wang A Z. Clinical indications for, and the future of, circulating tumor cells[J]. Adv. Drug Deliv. Rev., 2018, 125: 143−150.

[33] Tretyakova M S, Menyailo M E, Schegoleva A A, Bokova U A, Larionova I V, Denisov E V. Technologies for viable circulating tumor cell isolation[J]. Int. J. Mol. Sci., 2022, 23(24): 15979.

[34] Feng Z X, Wu J Y, Lu Y J, Chan Y T, Zhang C, Wang D, Luo D, Huang Y, Feng Y B, Wang N. Circulating tumor cells in the early detection of human cancers[J]. Int. J. Biol. Sci., 2022, 18(8): 3251−3265.

[35] Song Y, Tian T, Shi Y, Liu W L, Zou Y, Khajvand T, Wang S L, Zhu Z, Yang C Y. Enrichment and single-cell analysis of circulating tumor cells[J]. Chem. Sci., 2017, 8(3): 1736−1751.

[36] Akpe V, Kim T H, Brown C L, Cock I E. Circulating tumor cells: a broad perspective[J]. J. R. Soc. Interface, 2020, 17(168): 20200065.

[37] Bigall N C, Härtling T, Klose M, Klose M, Simon P, Eng L M, Eychmüller A. Monodisperse platinum nanospheres with adjustable diameters from 10 to 100 nm: synthesis and distinct optical properties[J]. Nano Lett., 2008, 8(12): 4588−4592.

基于铂纳米颗粒碰撞电化学用于快速检测乳腺癌 MCF-7 细胞

秦富星，李明珂，周汇龙，文　为，张修华，王升富，伍　珍*
湖北省小分子药物精准合成重点实验室，有机功能分子合成与应用教育部重点实验室，湖北大学化学化工学院，湖北 武汉 430062

摘要

癌症转移是全球癌症患者的主要死因，也是治疗癌症的主要挑战之一。循环肿瘤细胞（CTCs）在癌症转移过程中起着核心作用。但是，CTCs 在外周血中的含量极少，在实际样本中检测 CTCs 极具挑战性，故高效富集和早期检测 CTCs 对于及时诊断疾病至关重要。本工作利用免疫磁分离技术和脂质体信号放大策略构建了一种创新的、精密的用于检测 MCF-7 细胞（人类乳腺癌细胞）的 SNCE 生物传感器。以包埋铂纳米颗粒（Pt NPs）的脂质体为信号探针，以自制的金超微电极（Au UME）为工作电极。Pt NPs 与 UME 的每次有效碰撞都会产生可区分的阶梯型电流。根据细胞浓度与碰撞频率（单位时间内阶梯型电流数量）之间的关系，对 MCF-7 细胞进行了精确定量，实现了对 MCF-7 细胞的高灵敏度和特异性检测。该 SNCE 生物传感器线性范围为 10 cells·mL^{-1} 至 10^5 cells·mL^{-1}，检测限低至 5 cells·mL^{-1}。此外，在复杂样本中成功检测到 MCF-7 细胞，表面 SNCE 生物传感器在患者样本检测方面具有巨大潜力。

关键字：循环肿瘤细胞；单颗粒碰撞电化学；免疫磁分离；脂质体；铂纳米颗粒